

Benchmark of GW approaches for the GW100 testset

Fabio Caruso,[†] Matthias Dauth,[‡] Michiel J. van Setten,[¶] and Patrick Rinke^{*,§}

*Department of Materials, University of Oxford, Parks Road, Oxford OX1 3PH, United Kingdom,
Theoretical Physics IV, University of Bayreuth, D-95440 Bayreuth, Germany, Nanoscopic
Physics, Institute of Condensed Matter and Nanosciences, Université Catholique de Louvain,
1348 Louvain-la-Neuve, Belgium, and COMP/Department of Applied Physics, Aalto University,
P.O. Box 11100, Aalto FI-00076, Finland*

E-mail: patrick.rinke@aalto.fi

Abstract

For the recent GW100 test set of molecular ionization energies, we present a comprehensive assessment of different GW methodologies: fully self-consistent GW (scGW), quasi-particle self-consistent GW (qsGW), partially self-consistent GW_0 (sc GW_0), perturbative GW (G_0W_0) and optimized G_0W_0 based on the minimization of the deviation from the straight-line error (DSLE-minimized GW). We compare our GW calculations to coupled-cluster singles, doubles, and perturbative triples [CCSD(T)] reference data for GW100. We find scGW and qsGW ionization energies in excellent agreement with CCSD(T), with discrepancies typically smaller than 0.3 eV (scGW) respectively 0.2 eV (qsGW). For sc GW_0 and G_0W_0 the deviation

*To whom correspondence should be addressed

[†]Department of Materials, University of Oxford, Parks Road, Oxford OX1 3PH, United Kingdom

[‡]Theoretical Physics IV, University of Bayreuth, D-95440 Bayreuth, Germany

[¶]Nanososcopic Physics, Institute of Condensed Matter and Nanosciences, Université Catholique de Louvain, 1348 Louvain-la-Neuve, Belgium

[§]COMP/Department of Applied Physics, Aalto University, P.O. Box 11100, Aalto FI-00076, Finland

from CCSD(T) is strongly dependent on the starting point. We further relate the discrepancy between the GW ionization energies and CCSD(T) to the deviation from straight line error (DSLE). In DSLE-minimized GW calculations, the DSLE is significantly reduced, yielding a systematic improvement in the description of the ionization energies.

1 Introduction

Many-body perturbation theory provides an ideal framework for the first-principles study of electronic excitations in molecules and solids.¹ At variance with approaches based on density-functional theory (DFT),^{2,3} the description of electronic many-body interactions through the electron self-energy facilitates a seamless account of exact exchange and screening, which are essential to predict electronic excitations with quantitative accuracy.⁴⁻⁷ The GW approximation^{8,9} provides an ideal compromise between accuracy and computational cost and it has, thus, evolved into the state-of-the-art technique for the computation of ionization energies and band gaps in molecules and solids.⁵

GW calculations are typically based on first-order perturbation theory (G_0W_0),⁹ a procedure that introduces a spurious dependence of the results on the starting point, that is, the initial reference ground state the perturbation is applied to.^{6,10-13} The starting-point dependence may be reduced by resorting to partial self-consistent approaches,^{11,14} such as eigenvalue self-consistent GW or self-consistent GW_0 (sc GW_0), and it is completely eliminated in the self-consistent GW method (sc GW)^{15,16} – in which the Dyson equation is solved fully iteratively – and in quasi-particle self-consistent GW (qs GW).¹⁷⁻¹⁹ While sc GW implementations are still relatively rare,^{15,16,20-27} qs GW is now widely used.^{19,28-32} Moreover, with rare exceptions,²⁵ sc GW and qs GW are typically not implemented in the same code and have therefore not been systematically compared.

Given the various flavors of the self-consistent GW methodology, benchmark and validation are important instruments to (i) quantify the overall accuracy of GW calculations; (ii) reveal the effects of different forms of self-consistency; (iii) identify new ways to improve over existing techniques for quasiparticle calculations. The $GW100$ set provides an ideal test-case for addressing these

challenges.³³ This benchmark set is specifically designed to target the assessment of ionization energies and it is composed of 100 molecules of different bonding types, chemical compositions, and ionization energies.

In this manuscript, we present the ionization energies for the molecules of *GW*100 test set calculated with G_0W_0 , $scGW_0$, $scGW$, and $qsGW$. We analyse their behaviour in terms of the change in the electron density, the screening properties and the treatment of the kinetic energy. The accuracy of different *GW* approaches is established based on the comparison with coupled-cluster singles, doubles, and perturbative triples^{34–36} [CCSD(T)] energies obtained for the same geometries and basis sets.³⁷ Our study reveals that $scGW$ and $qsGW$ ionization energies differ on average by 0.3 eV and 0.15 eV from the CCSD(T) reference data, respectively. The discrepancy of G_0W_0 and $scGW_0$ from CCSD(T), on the other hand, is contingent on the starting point. For the *GW*100 set, we report an average starting-point dependence of 1 and 0.4 eV for G_0W_0 and $scGW_0$, respectively. Correspondingly, the starting point introduces an additional degree of freedom that allows one to improve the agreement with CCSD(T), e.g., by imposing the satisfaction of exact physical constraints. One of such constraint is the linearity of the total energy at fractional particle numbers.³⁸ The deviation from straight line error (DSLE) has been shown to lead to systematic errors in DFT, such as the tendency to overly localize or delocalize the electron density.^{39,40} Within the context of *GW* calculations, the DSLE may be minimized by varying the starting point. This procedure we refer to as the DSLE-minimized *GW* approach (DSLE-min).⁴¹ We show here that DSLE-min *GW* reduces the discrepancy with CCSD(T) for the *GW*100 set as compared to $scGW$ with an average absolute deviation slightly larger than that of $qsGW$ (0.26 eV, based on the def2-TZVPP basis set). Overall, our results provide a comprehensive assessment of the starting-point dependence, the accuracy of G_0W_0 and self-consistent *GW* methods, and suggest that the DSLE minimization may provide a strategy to improve the accuracy of the *GW* method at the cost of G_0W_0 calculations.

The manuscript is organized as follows. In Sec. 2 we review the basics of the *GW* method and self-consistency. The ionization energies for the *GW*100 test set are reported in Sec. 4, and

discussed in Sec. 5. DSLE-min GW results are discussed in Sec. 6. Conclusions and final remarks are presented in Sec. 7.

2 Methods

In the following, we give a brief introduction to the GW methodology employed throughout the manuscript: $scGW$, $scGW_0$, $qsGW$, perturbative G_0W_0 , and DSLE-min GW .

In the $scGW$ approach, the interacting Green's function G is determined through the iterative solution of Dyson's equation

$$G^{-1} = G_0^{-1} - [\Sigma - v_0 + \Delta v_H] \quad . \quad (1)$$

Δv_H denotes the change of the Hartree potential, which accounts for the density difference between G_0 and G , and v_0 is the exchange-correlation potential of the preliminary calculation. The non-interacting Green's function G_0 may be expressed as

$$G_0^\sigma(\mathbf{r}, \mathbf{r}', \omega) = \sum_n \frac{\psi_{n\sigma}(\mathbf{r}) \psi_{n\sigma}^*(\mathbf{r}')}{\omega - (\varepsilon_{n\sigma} - \mu) - i\eta \operatorname{sgn}(\mu - \varepsilon_{n\sigma})} \quad (2)$$

where μ is the Fermi energy, and η a positive infinitesimal. $\psi_{n\sigma}$ and $\varepsilon_{n\sigma}$ denote a set of single-particle orbitals and eigenvalues determined from an independent-particle calculation (e.g., Hartree-Fock, or DFT) for spin-channel σ . In the GW approximation, the self-energy Σ is given by

$$\Sigma_\sigma(\mathbf{r}, \mathbf{r}', \omega) = i \int \frac{d\omega'}{2\pi} G_\sigma(\mathbf{r}, \mathbf{r}', \omega + \omega') W(\mathbf{r}, \mathbf{r}', \omega') e^{i\omega\eta} \quad . \quad (3)$$

The screened Coulomb interaction W , in turn, is also determined from the solution of a Dyson-like

equation

$$W(\mathbf{r}, \mathbf{r}', \omega) = v(\mathbf{r}, \mathbf{r}') + \int d\mathbf{r}_1 d\mathbf{r}_2 v(\mathbf{r}, \mathbf{r}_1) \chi_0(\mathbf{r}_1, \mathbf{r}_2, \omega) W(\mathbf{r}_2, \mathbf{r}', \omega) \quad , \quad (4)$$

where $v(\mathbf{r}, \mathbf{r}') = |\mathbf{r} - \mathbf{r}'|^{-1}$ is the bare Coulomb interaction. The polarizability χ_0 is most easily expressed on the time axis τ

$$\chi_0(\mathbf{r}, \mathbf{r}', \tau) = -i \sum_{\sigma} G_{\sigma}(\mathbf{r}, \mathbf{r}', \tau) G_{\sigma}(\mathbf{r}', \mathbf{r}, -\tau) \quad . \quad (5)$$

and is Fourier transformed to the frequency axis before it is used in Eq. (??).

The structure of Eqs. (??)-(??) reveals the self-consistent nature of the *GW* approximation. Due to the interdependence of G , χ_0 , W , and Σ , Eqs. (??)-(??) need to be solved iteratively until the satisfaction of a given convergence criterion.¹⁶ We denote the procedure in which Eqs. (??)-(??) are solved fully self-consistently as *scGW*. Recent studies have revealed that Hedin's equations may exhibit multiple-solution behaviour.⁴²⁻⁴⁷ For closed shell molecules we have not yet observed multiple solutions. Moreover, it has been shown that, if self-consistency is achieved through the solution of the Dyson equation, as in this work, the self-consistent loop converges to the unique physical solution.⁴⁶

In *scGW*₀ the screened interaction W is evaluated only once using orbitals and eigenvalues from an independent-particle calculation. The Dyson equation is thus solved iteratively updating G and Σ at each step, but keeping W_0 fixed. In *scGW* and *scGW*₀, the physical properties of the system – such as, e.g., the total energy,^{20,21,48-50} the electron density,⁵¹ and the ionization energy^{15,23} – may be extracted directly from the self-consistent Green's function by means of the spectral function

$$A(\omega) = -\frac{1}{\pi} \int d\mathbf{r} \lim_{\mathbf{r}' \rightarrow \mathbf{r}} \text{Im} G(\mathbf{r}, \mathbf{r}', \omega) \quad . \quad (6)$$

As an example, we report in Fig. 1 the spectral function of the adenine nucleobase (C₅H₅N₅O)

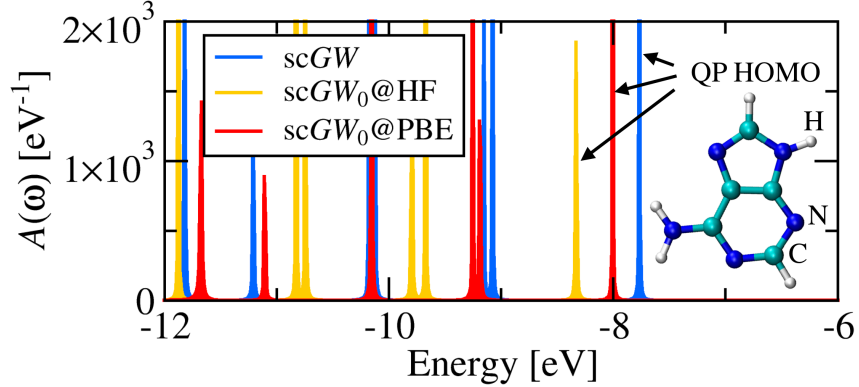


Figure 1: Spectral function of the adenine nucleobase, for which the molecular geometry is shown, obtained from $scGW$, $scGW_0@HF$, and $scGW_0@PBE$ using the def2-TZVPP basis set.⁵² The quasiparticle HOMO is indicated by arrows.

evaluated using $scGW$, $scGW_0@HF$, and $scGW_0@PBE$. For each approach, the energy of the quasiparticle HOMO is given by the position of the highest energy peak, indicated by arrows in Fig. 1. We note that $scGW_0$ still exhibits a dependence on the starting point, which stems from the non-self-consistent treatment of W , whereas $scGW$ is completely independent of the initial reference calculation.¹⁵

In the G_0W_0 approach, the quasiparticle energies ϵ^{QP} are evaluated as a first-order perturbative correction to a set of single-particle (SP) eigenvalues ϵ^{SP} [obtained, for instance, from DFT]

$$\epsilon_{n\sigma}^{QP} = \epsilon_{n\sigma}^{SP} + \langle \psi_n^\sigma | \Sigma(\epsilon_{n\sigma}^{QP}) - v_0 | \psi_n^\sigma \rangle \quad . \quad (7)$$

Owing to the perturbative nature of Eq. (7), one would expect a pronounced dependence of $\epsilon_{n\sigma}^{QP}$ on the starting point, that is, on the set of eigenvalues $\epsilon_{n\sigma}^{SP}$ and orbitals $\psi_{n\sigma}$. To benchmark the starting point dependence for the $GW100$ test set we consider hereafter two different starting points: Hartree-Fock and the Perdew-Burke-Ernzerhof⁵³ (PBE) generalized gradient approximation to DFT. We explicitly denote the starting-point dependence by adopting the notation *method@starting point* (e.g., $G_0W_0@PBE$).

In the $qsGW$ self-consistency treatment the Green's function keeps the analytic structure of a

non-interacting Green's function (omitting spin indices for brevity)

$$G_0^{\text{qsGW}}(\mathbf{r}, \mathbf{r}', \omega) = \sum_n \frac{\psi_n^{\text{QP}}(\mathbf{r}) \psi_n^{*\text{QP}}(\mathbf{r}')}{\omega - (\epsilon_n^{\text{QP}} - \mu) - i\eta \text{sgn}(\mu - \epsilon_n^{\text{QP}})}. \quad (8)$$

The quasi-particle orbitals and energies are iteratively updated solving the quasi-particle equation applying a linear mixing scheme.^{17–19} The QP-orbitals of the $(i+1)$ th iteration $\psi_n^{(i+1)}(\mathbf{r})$ are expressed in terms of the orbitals of the previous iteration

$$\psi_n^{(i+1)}(\mathbf{r}) = \sum_{\underline{n}} \mathcal{A}_{n\underline{n}}^{(i+1)} \psi_{\underline{n}}^{(i)}(\mathbf{r}). \quad (9)$$

In the reference basis $\psi_{\underline{n}}^{(i)}(\mathbf{r})$ Eq. (??) takes the form of an eigenvalue problem

$$\sum_{\underline{n}} \mathcal{A}_{n\underline{n}}^{(i+1)} \left[\int d\mathbf{r} d\mathbf{r}' \psi_{\underline{n}}^{(i)}(\mathbf{r}) (H_0[G_0^{(i)}] \delta(\mathbf{r} - \mathbf{r}') + \tilde{\Sigma}(\mathbf{r}, \mathbf{r}')) \psi_{\underline{n}}^{(i)}(\mathbf{r}') \right] = \epsilon_{n'}^{\text{QP}(i+1)} \mathcal{A}_{n'n}^{(i+1)} \quad (10)$$

where $H_0[G_0^{\text{qsGW}}]$ is the single-particle part of the Hamiltonian evaluated with the electron density generated by G_0^{qsGW} . The self-energy matrix is approximated as static and Hermitian

$$\tilde{\Sigma}_{nn'} = \frac{1}{2} (\Sigma_{nn'}(\epsilon_n) + \Sigma_{nn'}(\epsilon_{n'})). \quad (11)$$

The diagonalization of Eq. (10) updates $\epsilon_{n'}^{\text{QP}(i+1)}$ and $\mathcal{A}_{n'n}^{(i+1)}$. With these new orbitals, the wave functions at iteration $i+1$ ($\psi_n^{\text{QP}(i+1)}(\mathbf{r})$) are constructed via Eq. (??). The orbitals become orthonormal by construction due to the hermiticity of the operators in Eq. (10).

qsGW is closely related to $G_0 W_0$ in the sense that in each cycle of the self-consistent solution the Green's function is a non-interacting G_0 . The final result was shown to be independent of the starting point,¹⁹ but both the stability of the iterative cycle and the rate of convergence can be greatly improved by using an optimal starting point. In addition, it was found that a simple iteration scheme may not always converge. In practice linear mixing scheme is applied. In qsGW

the orbital energies are directly available via Eq. (10).

Beside *scGW*, *scGW*₀, and *qsGW*, other approximate self-consistent *GW* approaches have been investigated in the past, such as eigenvalue self-consistent *GW*,^{11,14,54,55} and *GW*+COHSEX.^{13,56} These will not be discussed in this article.

Among the different flavors of *GW* calculations, the starting-point dependence is most pronounced in *G*₀*W*₀, since both *G*₀ and *W*₀ depend explicitly on the initial set of orbitals and eigenvalues. Yet, this ambiguity also provides a means to improve the accuracy of *G*₀*W*₀, by seeking the optimal starting point that leads to the satisfaction of exact physical constraints. A prominent example is the piecewise linearity of the total energy.⁵⁷ Usually approximate theories do not automatically exhibit a linearly changing total energy under fractional electron removal (or addition) but instead produce a DSLE. If the total energy were a linear function of the fractional particle number, the ionization energy of the neutral system would be equal to the electron affinity of the cation (EA_c).^{40,58} Identifying the ionization energy with the *G*₀*W*₀ quasiparticle HOMO and EA_c with the LUMO of the cationic system, one may thus define the DSLE as⁴¹

$$\Delta_{\text{DSLE}} \equiv \epsilon_{\text{HOMO}}^{\text{QP}} - \epsilon_{\text{LUMO,c}}^{\text{QP}}. \quad (12)$$

This definition can be applied to approximately quantify the DSLE in the *GW* method without explicitly invoking the total energy at fractional particle numbers. Furthermore, the minimization of Δ_{DSLE} in *G*₀*W*₀ calculations allows one to find a starting point that minimizes or completely eliminates the DSLE. We here adopt the DSLE-min *GW* approach proposed in Ref. 41 which is based on these concepts. For the DSLE-min procedure we utilize starting points from PBE-based hybrid (PBEh) functionals⁵⁹ with an adjustable fraction α of Hartree-Fock exchange and evaluate Eq. (??) with the *G*₀*W*₀@PBEh(α) quasiparticle energies. We then identify the optimal starting point with the very α that leads to a minimization of Δ_{DSLE} .

The coupled cluster singles, doubles, and perturbative triples [CCSD(T)]^{34–36} approach is often regarded as the *gold standard* among the quantum chemistry methods as it yields results that

approach chemical accuracy for a variety of physical/chemical properties, such as binding energies and atomization energies. CCSD(T) values are thus particularly suitable to unambiguously establish the accuracy of *GW* approaches for the ionization energies. In the following, our calculated ionization energies are compared to reference values from CCSD(T),³⁷ whereby the ionization energy has been obtained as a total energy difference between the ionized and neutral molecules. The comparison to CCSD(T) is here preferred to experimental data as it allows us to focus on the effects of exchange and correlation. We can therefore safely ignore the effects of temperature, nuclear vibrations, and interaction with the environment, which affect experimental ionization energies.⁶⁰ The CCSD(T) calculations of Ref. 37 used the molecular geometries of the *GW*100 test set,³³ and are therefore suitable to be compared with our calculations, in which the same geometries were employed. Additional details on the CCSD(T) calculations may be found in Ref. 37.

3 Computational details

Our G_0W_0 , DSLE-min *GW*, and sc*GW* calculations have been performed with the `FHI-aims` code,^{61–63} whereas qs*GW* calculations have been performed using a local version of the `TURBOMOLE`⁶⁴ code. For G_0W_0 , DSLE-min *GW*, and sc*GW* the frequency dependence is treated on the imaginary frequency axis and the quasiparticle energies are extracted by performing an analytic continuation based on Padé approximants. Similarly to Ref. 33, for G_0W_0 and DSLE-min *GW* the parametrization of the analytic continuation employed 200 imaginary frequency points on a Gauss-Legendre grid and 16 poles for the Padé approximant method. The qs*GW* calculations were performed directly in real frequency by exploiting the full analytic structure of *G* and *W* as described in Ref. 19,65. Our sc*GW* calculations used the same computational parameters as Ref. 15,16 for the frequency dependence. At variance with Ref. 33, no basis set extrapolation scheme has been employed in this work. Additional details on the numerical implementations of G_0W_0 , sc*GW*, and sc*GW*₀ in `FHI-aims`^{15,16,63} and the qs*GW* implementation in `TURBOMOLE`^{19,65} can be found elsewhere. All calculations use the same parameters reported in Ref. 33 for the

resolution-of-identity, and the real-space grids. To enable the direct comparison with reference values from CCSD(T), we used the Gaussian def2-TZVPP basis sets.⁵² In FHI-aims the Gaussian basis function are numerically tabulated and are treated as numerical orbitals. We refer to Ref. 33 for detailed convergence tests for this procedure. For the DSLE-min method, basis set converged calculations for the quasiparticle energies have been performed using the Tier 4 basis sets augmented by Gaussian aug-cc-pV5Z basis functions (Tier 4⁺).⁶³ To facilitate the comparison with CCSD(T), we also report DSLE-min quasiparticle energies obtained with def2-TZVPP basis sets.

We use the same geometries as in Ref. 33.¹ We assume zero electronic temperature and the effects of nuclear vibrations are ignored. All ionization energies are vertical and do not include any relativistic corrections.

4 Ionization energies for the GW100 set

The GW100 test set consists of 100 atoms and molecules which have been selected to span a broad range of chemical bonding situations, chemical compositions, and ionization energies. Due to the absence of all-electron def2-TZVPP basis sets for fifth-row elements, we exclude Xe, Rb₂, Ag₂, and the iodine-containing compounds (I₂, C₂H₃I, Cl₄, and AlI₃). For the remaining 93 member of GW100 we can then conduct a meaningful comparison with CCSD(T) reference data.

As discussed in Ref. 33, many molecules of the GW100 testset have positive LUMO energies (that is, negative electron affinities), which makes them unsuitable for a systematic assessment of electron affinities since experimental data for such compounds is difficult to obtain. Moreover, CCSD(T) reference data is presently also not available for the LUMOs in the GW100 testset.³⁷ For these reasons, we focus here on the first vertical ionization energy, for which experimental and CCSD(T) reference data are available. An assessment of GW methods for electron affinities may be found in Ref. 13. In table 1, we report the ionization energies for this subset of GW100 calculated

¹Experimental geometries have been employed whenever available, otherwise molecular geometries are optimized within the PBE approximation for the exchange-correlation functional using the def2-QZVP basis set. More details on the strategy adopted for selecting the compounds of the GW100 set and their geometries are given in Ref. 33.

with qsGW, scGW, scGW₀@HF, and scGW₀@PBE and def2-TZVPP basis sets. For comparison, we also report the CCSD(T) ionization energies from Ref. 37.

Table 1: Vertical ionization energies for the GW100 test set calculated with qsGW, scGW, scGW₀@HF, scGW₀@PBE, and DSLE-minimized G_0W_0 (DSLE-min) and def2-TZVPP basis sets. Basis set converged DSLE-minimized G_0W_0 calculations employ Tier 4 basis sets augmented by Gaussian aug-cc-pV5Z basis functions, denoted as DSLE-min (T4+). For comparison, we also report CCSD(T) values from Ref.³⁷ All values are in eV.

	Name	Formula	qsGW	scGW	scGW ₀ @HF	scGW ₀ @PBE	DSLE-min	DSLE-min (T4+)	CCSD(T)
1	Helium	He	-24.43	-24.44	-24.47	-24.01	-	-	-24.51
2	Neon	Ne	-21.62	-21.40	-21.49	-20.84	-20.82	-20.22	-21.32
3	Argon	Ar	-15.53	-15.26	-15.50	-15.18	-15.34	-15.27	-15.54
4	Krypton	Kr	-13.74	-13.65	-13.88	-13.62	-13.62	-13.75	-13.94
6	Hydrogen	H ₂	-16.22	-16.18	-16.27	-15.98	-	-	-16.40
7	Lithium dimer	Li ₂	-5.34	-4.96	-5.15	-5.02	-5.00	-5.05	-5.27
8	Sodium dimer	Na ₂	-5.02	-4.63	-4.80	-4.74	-4.87	-4.93	-4.95
9	Sodium tetramer	Na ₄	-4.25	-3.85	-4.09	-3.99	-4.18	-4.27	-4.23
10	Sodium hexamer	Na ₆	-4.41	-3.94	-4.25	-4.16	-4.31	-4.40	-4.35
11	Dipotassium	K ₂	-4.08	-3.73	-3.90	-3.86	-3.96	-4.10	-4.06
13	Nitrogen	N ₂	-16.01	-15.44	-15.84	-15.32	-15.49	-15.75	-15.57
14	Phosphorus dimer	P ₂	-10.40	-9.73	-10.20	-10.01	-10.30	-10.52	-10.47
15	Arsenic dimer	As ₂	-9.62	-9.00	-9.48	-9.34	-9.52	-9.82	-9.78
16	Fluorine	F ₂	-16.33	-15.78	-16.17	-15.50	-15.56	-15.76	-15.71
17	Chlorine	Cl ₂	-11.52	-11.07	-11.47	-11.13	-11.36	-11.55	-11.41
18	Bromine	Br ₂	-10.54	-10.23	-10.58	-10.30	-10.31	-10.77	-10.54
20	Methane	CH ₄	-14.56	-14.28	-14.50	-14.14	-14.20	-14.35	-14.37
21	Ethane	C ₂ H ₆	-12.99	-12.62	-12.92	-12.55	-12.60	-12.75	-13.04
22	Propane	C ₃ H ₈	-12.35	-11.95	-12.30	-11.92	-12.03	-12.18	-12.05
23	Butane	C ₄ H ₁₀	-11.89	-11.46	-11.85	-11.46	-11.73	-11.88	-11.57
24	Ethylene	C ₂ H ₄	-10.63	-10.14	-10.45	-10.24	-10.40	-10.60	-10.67
25	Acetylene	C ₂ H ₂	-11.53	-10.89	-11.23	-10.98	-11.17	-11.43	-11.42
26	tetracarbon	C ₄	-11.45	-10.68	-11.21	-10.87	-10.87	-11.07	-11.26
27	Cyclopropane	C ₃ H ₆	-11.13	-10.62	-10.98	-10.66	-10.77	-11.00	-10.87
28	Benzene	C ₆ H ₆	-9.38	-8.73	-9.20	-8.97	-9.12	-9.34	-9.29
29	Cyclooctatetraene	C ₈ H ₈	-9.30	-7.81	-8.33	-8.04	-8.21	-8.44	-8.35
30	Cyclopentadiene	C ₅ H ₆	-8.73	-8.10	-8.54	-8.29	-8.47	-8.69	-8.68
31	Vinyl fluoride	C ₂ H ₃ F	-10.64	-10.11	-10.46	-10.16	-10.36	-10.59	-10.55
32	Vinyl chloride	C ₂ H ₃ Cl	-10.09	-9.63	-10.02	-9.72	-9.92	-10.14	-10.09
33	Vinyl bromide	C ₂ H ₃ Br	-9.33	-8.82	-9.19	-8.94	-9.06	-9.32	-9.27
35	Carbon tetrafluoride	CF ₄	-16.77	-16.34	-16.75	-15.89	-15.84	-15.78	-16.30
36	Carbon tetrachloride	CCl ₄	-11.63	-11.16	-11.69	-11.18	-11.46	-11.57	-11.56
37	Carbon tetrabromide	CBr ₄	-10.57	-10.10	-10.59	-10.16	-10.33	-10.59	-10.46
39	Silane	SiH ₄	-13.04	-12.74	-13.00	-12.55	-12.66	-12.88	-12.80
40	Germane	GeH ₄	-12.81	-12.40	-12.67	-12.28	-12.41	-12.55	-12.50
41	Disilane	Si ₂ H ₆	-10.88	-10.46	-10.82	-10.45	-10.48	-10.75	-10.65
42	Pentasilane	Si ₅ H ₁₂	-9.56	-9.04	-9.50	-9.10	-9.18	-9.32	-9.27
43	Lithium hydride	LiH	-8.00	-7.88	-7.97	-7.45	-6.48	-6.71	-7.96
44	Potassium hydride	KH	-6.17	-6.02	-6.17	-5.52	-5.65	-5.63	-6.13
45	Borane	BH ₃	-13.52	-13.22	-13.42	-13.05	-13.17	-13.30	-13.28
46	Diborane(6)	B ₂ H ₆	-12.58	-12.23	-12.54	-12.09	-12.17	-12.30	-12.26
47	Ammonia	NH ₃	-11.08	-10.76	-10.97	-10.59	-10.59	-10.78	-10.81

Continues on next page

Table 1 continued

	Name	Formula	qsGW	scGW	scGW ₀ @HF	scGW ₀ @PBE	DSLE-min	DSLE-min (T4+)	CCSD(T)
48	Hydrogen azide	HN ₃	-10.91	-10.24	-10.69	-10.38	-10.61	-10.89	-10.68
49	Phosphine	PH ₃	-10.65	-10.24	-10.53	-10.28	-10.39	-10.60	-10.52
50	Arsine	AsH ₃	-10.50	-10.10	-10.39	-10.17	-10.24	-10.49	-10.40
51	Hydrogen sulfide	SH ₂	-10.39	-9.97	-10.26	-10.02	-10.15	-10.38	-10.31
52	Hydrogen fluoride	FH	-16.33	-16.11	-16.26	-15.71	-15.63	-15.64	-16.03
53	Hydrogen chloride	ClH	-12.65	-12.28	-12.55	-12.27	-12.41	-12.57	-12.59
54	Lithium fluoride	LiF	-11.52	-11.34	-11.50	-10.59	-10.66	-10.85	-11.32
55	Magnesium fluoride	F ₂ Mg	-13.99	-13.77	-13.97	-13.05	-12.87	-13.00	-13.71
56	Titanium fluoride	TiF ₄	-15.75	-15.55	-16.15	-14.98	-14.80	-15.19	-15.48
57	Aluminum fluoride	AlF ₃	-15.69	-15.40	-15.68	-14.83	-14.59	-14.75	-15.46
58	Fluoroborane	BF	-11.13	-10.64	-10.94	-10.56	-10.82	-10.98	-11.09
59	Sulfur tetrafluoride	SF ₄	-12.98	-12.47	-12.95	-12.36	-12.51	-12.73	-12.59
60	Potassium bromide	BrK	-8.15	-7.88	-8.12	-7.72	-7.84	-8.25	-8.13
61	Gallium monochloride	GaCl	-9.80	-9.35	-9.69	-9.49	-9.62	-9.93	-9.77
62	Sodium chloride	NaCl	-9.07	-8.79	-9.03	-8.51	-8.79	-9.03	-9.03
63	Magnesium chloride	MgCl ₂	-11.64	-11.39	-11.70	-11.24	-11.22	-11.39	-11.67
65	Boron nitride	BN	-11.79	-11.06	-11.58	-11.27	-11.19	-11.81	-11.89
66	Hydrogen cyanide	NCH	-13.65	-13.15	-13.51	-13.20	-13.47	-13.72	-13.87
67	Phosphorus mononitride	PN	-11.93	-11.56	-12.03	-11.60	-11.60	-11.84	-11.74
68	Hydrazine	H ₂ NNH ₂	-10.08	-9.63	-9.93	-9.52	-9.53	-9.75	-9.72
69	Formaldehyde	H ₂ CO	-11.22	-10.82	-11.15	-10.67	-10.77	-11.02	-10.84
70	Methanol	CH ₄ O	-11.46	-11.07	-11.36	-10.86	-10.94	-11.19	-11.04
71	Ethanol	C ₂ H ₆ O	-11.07	-10.69	-11.05	-10.51	-10.59	-10.84	-10.69
72	Acetaldehyde	C ₂ H ₄ O	-10.62	-10.20	-10.59	-10.03	-10.10	-10.36	-10.21
73	Ethoxy ethane	C ₄ H ₁₀ O	-10.23	-9.81	-10.27	-9.67	-9.77	-10.02	-9.82
74	formic acid	CH ₂ O ₂	-11.78	-11.42	-11.80	-11.19	-11.29	-11.57	-11.42
75	Hydrogen peroxide	HOOH	-11.98	-11.55	-11.90	-11.38	-11.42	-11.69	-11.59
76	Water	H ₂ O	-12.91	-12.59	-12.78	-12.32	-12.26	-12.45	-12.57
77	Carbon dioxide	CO ₂	-14.07	-13.55	-13.95	-13.45	-13.61	-13.91	-13.71
78	Carbon disulfide	CS ₂	-10.04	-9.45	-9.95	-9.69	-9.89	-10.14	-9.98
79	Carbon oxysulfide	OCS	-11.33	-10.72	-11.17	-10.88	-11.08	-11.35	-11.17
80	Carbon oxyselelide	OCS _e	-10.60	-10.00	-10.42	-10.19	-10.29	-10.62	-10.79
81	Carbon monoxide	CO	-14.55	-13.95	-14.43	-13.90	-14.21	-14.44	-14.21
82	Ozone	O ₃	-13.21	-12.54	-13.16	-12.57	-12.24	-12.49	-12.55
83	Sulfur dioxide	SO ₂	-12.54	-12.05	-12.54	-12.06	-12.21	-12.55	-13.49
84	Beryllium monoxide	BeO	-10.11	-9.77	-10.01	-9.58	-9.40	-9.68	-9.94
85	Magnesium monoxide	MgO	-8.30	-7.97	-8.27	-7.72	-7.48	-7.60	-7.49
86	Toluene	C ₇ H ₈	-9.00	-8.35	-8.83	-8.60	-8.74	-8.96	-8.90
87	Ethylbenzene	C ₈ H ₁₀	-8.97	-8.30	-8.80	-8.55	-8.68	-8.91	-8.85
88	Hexafluorobenzene	C ₆ F ₆	-9.91	-9.48	-10.08	-9.66	-9.96	-10.23	-9.93
89	Phenol	C ₆ H ₅ OH	-8.82	-8.19	-8.67	-8.39	-8.52	-8.78	-8.70
90	Aniline	C ₆ H ₅ NH ₂	-8.12	-7.51	-7.99	-7.69	-7.83	-8.09	-7.99
91	Pyridine	C ₅ H ₅ N	-9.76	-9.11	-9.58	-9.37	-9.53	-9.76	-9.66
92	Guanine	C ₅ H ₅ N ₅ O	-7.95	-7.49	-8.06	-7.71	-7.88	-8.18	-8.03
93	Adenine	C ₅ H ₅ N ₅ O	-8.41	-7.77	-8.33	-8.00	-8.16	-8.45	-8.33
94	Cytosine	C ₄ H ₅ N ₃ O	-8.99	-8.38	-8.93	-8.47	-8.63	-8.92	-9.51
95	Thymine	C ₅ H ₆ N ₂ O ₂	-9.30	-8.69	-9.25	-8.83	-9.01	-9.28	-9.08
96	Uracil	C ₄ H ₄ N ₂ O ₂	-9.74	-9.12	-9.66	-9.22	-9.41	-9.69	-10.13
97	Urea	CH ₄ N ₂ O	-10.45	-10.02	-10.45	-9.81	-10.13	-10.44	-10.05
99	Copper dimer	Cu ₂	-7.52	-6.98	-7.23	-7.29	-7.15	-7.57	-7.57
100	Copper cyanide	NCCu	-10.97	-10.54	-11.13	-10.26	-10.38	-10.50	-10.85

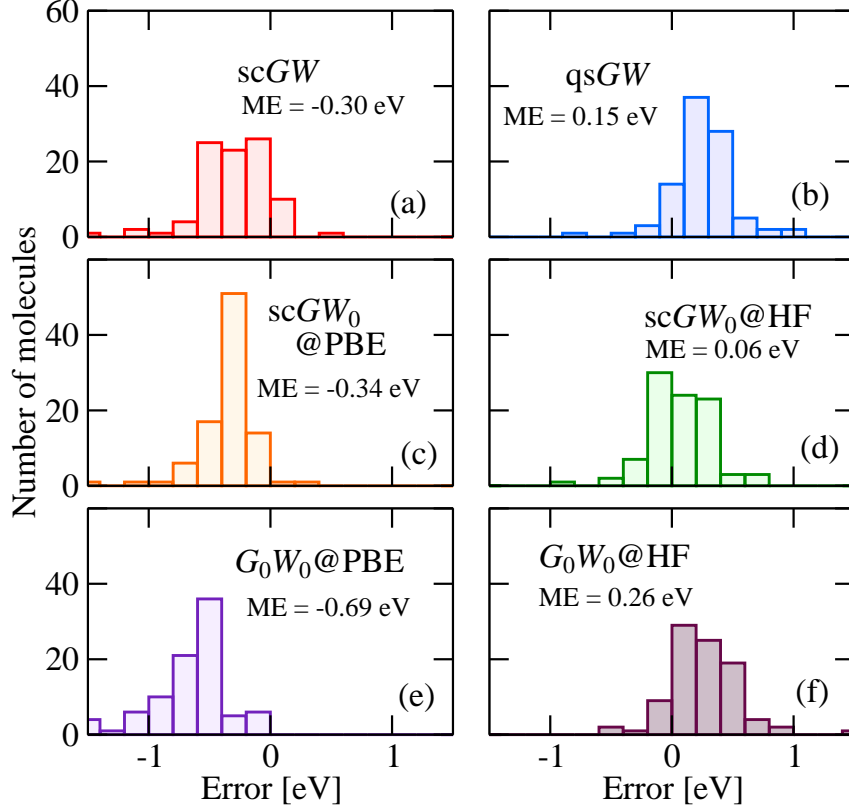


Figure 2: Error distribution [defined as the difference to CCSD(T) reference energies from Ref. 37] for the ionization energies of the *GW*100 test set evaluated using (a) *scGW*, (b) *qsGW*, (c) *scGW*₀@PBE, (d) *scGW*₀@HF, (e) *G*₀*W*₀@PBE, and (f) *G*₀*W*₀@HF and def2-TZVPP basis sets. The mean error (ME) for each method is listed in the corresponding panel.

5 Comparison of *GW* Methods

To quantify the deviation from CCSD(T) calculations, we analyse the error $\Delta \equiv \epsilon_{\text{CCSD(T)}}^{\text{HOMO}} - \epsilon_{\text{QP}}^{\text{HOMO}}$ and the absolute error $\Delta_{\text{abs}} \equiv |\epsilon_{\text{CCSD(T)}}^{\text{HOMO}} - \epsilon_{\text{QP}}^{\text{HOMO}}|$. In Fig. 2, we report the error distribution for the molecules of the *GW*100 test set, whereas the absolute error is reported in Fig. 3.

5.1 *scGW* vs *qsGW*

We start by considering the *scGW* and *qsGW* approaches. At variance with *G*₀*W*₀ and *scGW*₀, the *scGW* ionization energies are independent of the starting point.^{15,16} Any deviations between *scGW* and CCSD(T) can then be attributed to intrinsic limitations of the *GW* approximation (i.e. missing vertex corrections) rather than the artificial starting-point dependence introduced by perturbation

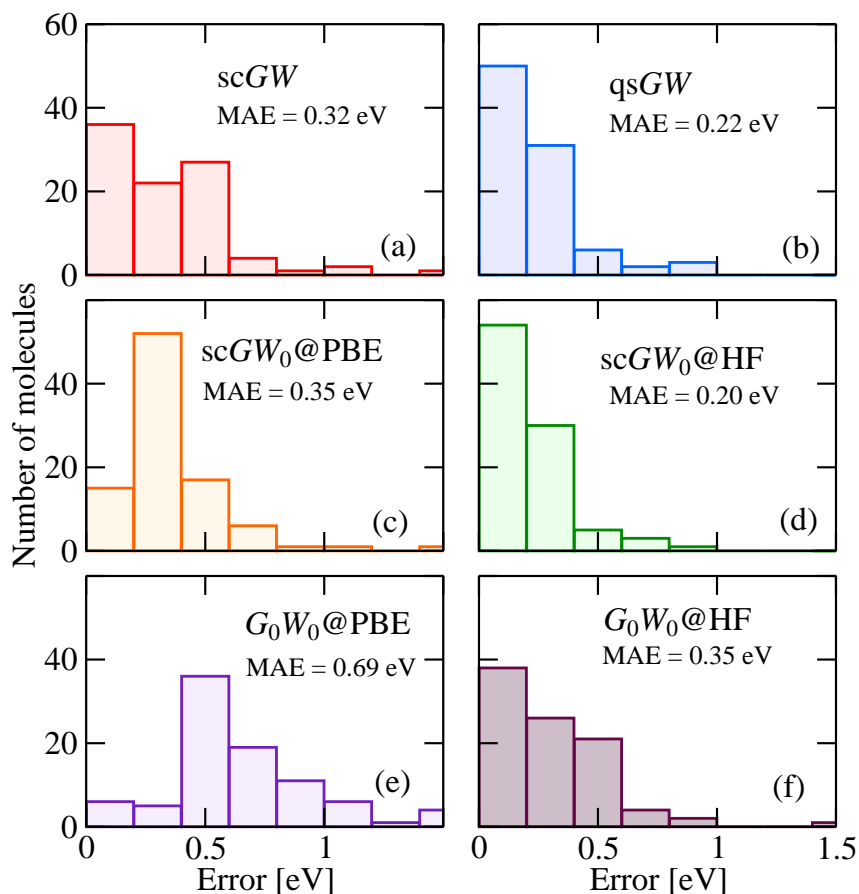


Figure 3: Absolute error distribution (defined similarly to Fig. 2) for the ionization energies of the GW100 test set evaluated using (a) *scGW*, (b) *qsGW*, (c) *scGW*₀@PBE, (d) *scGW*₀@HF, (e) *G*₀*W*₀@PBE, and (f) *G*₀*W*₀@HF and def2-TZVPP basis sets. The mean absolute error (MAE) for each method is listed in the corresponding panel.

theory or approximate self-consistent procedures. The *qsGW* ionization energies of molecules have also been reported to be independent of the starting point.¹⁹ However, for some solids, a dependence on the starting point has been observed.⁶⁶

Our calculations reveal that *qsGW* overestimates the ionization potentials in our test set by 0.15 eV on average [Fig. 2 (b)], whereas *scGW* underestimates them by 0.3 eV [Fig. 2 (a)]. *qsGW* exhibits a MAE of ~ 0.22 eV [Fig. 3 (b)] and it thus yields quasiparticle energies in slightly better agreement with CCSD(T) than *scGW* [MAE= 0.32 eV, Fig. 3 (a)]. Overall, *scGW* and *qsGW* ionization energies differ on average by 0.45 eV, revealing that different forms of self-consistency may affect significantly the value of the quasiparticle energies and the corresponding agreement with experiment. In the following we explore four different potential explanations.

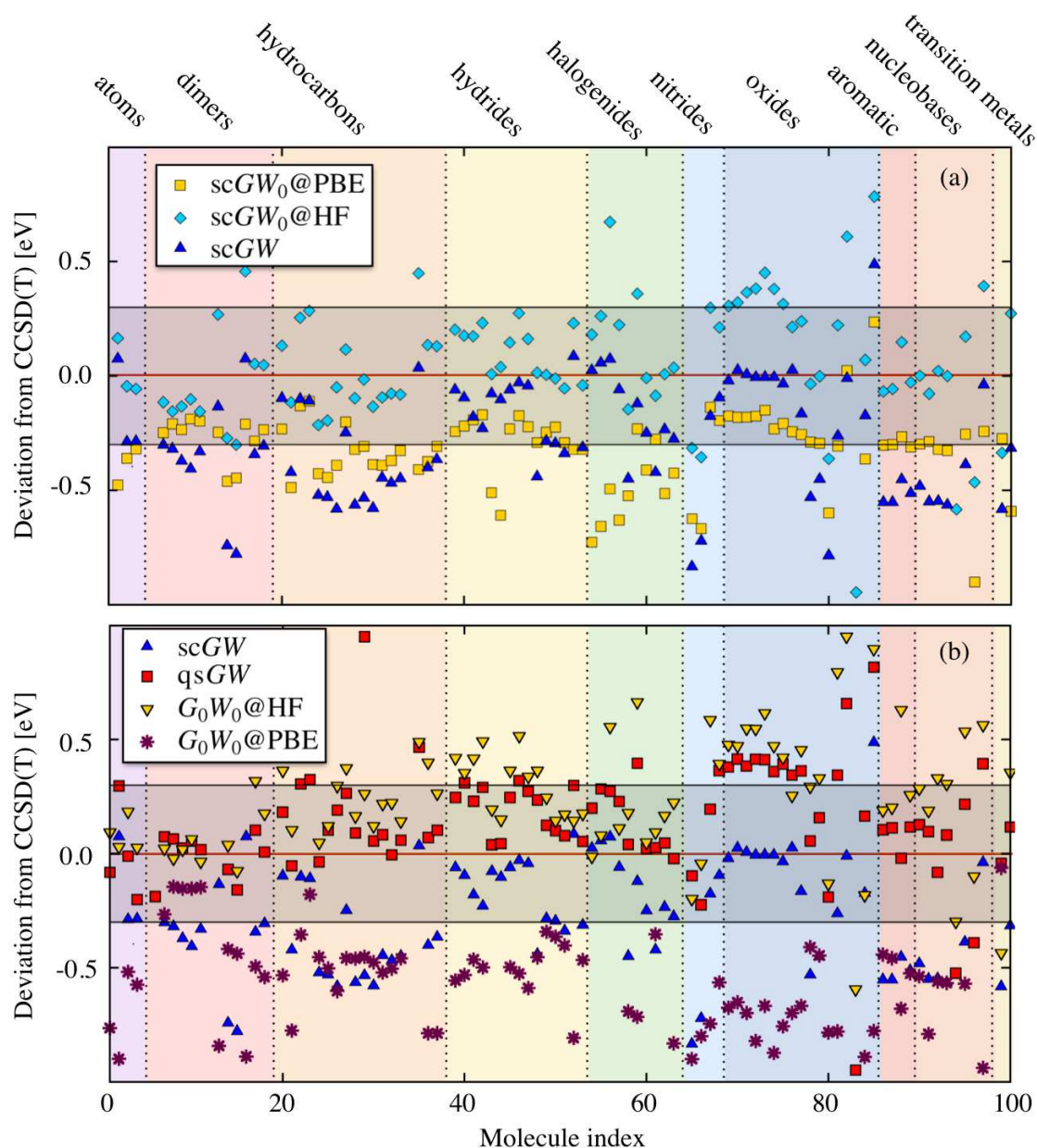


Figure 4: Deviation between the CCSD(T) reference ionization energies and our first-principles calculations obtained using (a) scGW, scGW₀@PBE, and scGW₀@HF, and (b) scGW, qsGW, G₀W₀@PBE, and G₀W₀@HF and def2-TZVPP basis sets. Only compounds with ionization energies that differ from CCSD(T) by less than 1 eV are included. Vertical dotted lines denotes the separation between different subgroups of the GW100 test set and coincide with the horizontal separation lines of table 1. The separation in subgroups (as well as the name attributed to each subgroup) is a guide to the eye, but not necessarily representative of the chemical compositions of each compound. Points falling within the horizontal shaded area differ by less the 0.3 eV from CCSD(T).

5.1.1 Screening properties

While it is expected that different forms of self-consistency lead to different results, the magnitude of the difference is surprising. At first glance, *scGW* and *qsGW* should be similar since in both approaches the quasiparticle energies enter the denominator of the Green's function. For both approaches we would therefore expect underscreening, due to the inverse dependence of the magnitude of screening on the energy difference between the lowest unoccupied and the highest occupied state in *GW*. In a beyond-*GW* treatment this underscreening due to the large quasiparticle gap would be compensated by vertex corrections, such as ladder diagrams.^{30,67} Without this compensation, the underscreening due to the too large quasiparticle gap in *W* would lead to an overestimation of ionization energies and quasiparticle energies that resemble those of $G_0W_0@HF$, which is also based on an underscreened W_0 due to the large HOMO-LUMO gap in HF. For *qsGW* we indeed observe this resemblance with $G_0W_0@HF$ in Fig. 2 and 3, which results in the aforementioned slight average overestimation of ionization energies compared to CCSD(T). The small reduction of the ionization energies by 0.09 eV in going from $G_0W_0@HF$ to *qsGW* can therefore be attributed to a reduction of the underscreening due to the fact that the *qsGW* gap is smaller than the HF gap and to density changes that we will discuss in the following.

The corresponding ionization-energy histogram for *scGW* is closer to $scGW_0@PBE$ and $G_0W_0@PBE$ than to $G_0W_0@HF$, with a concomitant underestimation of the CCSD(T) reference data. This observation is consistent with previous *scGW* calculations for molecules^{11,13,15,16,25,51,68} that observed a similar underestimation of the ionization potential. Also in *scGW* the HOMO-LUMO gaps is smaller than in $G_0W_0@HF$ and smaller than in *qsGW*. *scGW* therefore underscreens less than *qsGW* and we attribute part of the 0.45 eV average deviation between *qsGW* and *scGW* to this difference in screening.

5.1.2 Spectral-weight transfer

For solids, a spectral-weight transfer from the main quasiparticle peaks to satellites has been reported for *scGW* calculations of the homogeneous electron gas.⁶⁹ Schematically, the self-consistent

Green’s function can be written as $G = ZG_{qp} + \bar{G}$, where Z is the spectral weight of the quasiparticle peak G_{qp} and \bar{G} the incoherent part of the spectral function. In *qsGW* Z is equal to one and \bar{G} is zero.^{19,70} Conversely, for *scGW* Z is smaller than one and \bar{G} larger than zero, as spectral weight is transferred from G_{qp} to \bar{G} . This spectral weight transfer leads to an additional underscreening and an overestimation of band gaps in solids.^{22,27,71}

For small molecules there are no continuum states or collective excitations that could be excited at valence energies.⁴⁹ The *scGW* spectral functions therefore are sharply peaked around the quasiparticle energies and the spectrum exhibits no signature of an incoherent background in the valence energy region⁴⁹ as show in Fig. 1. We would thus not expect any additional underscreening due to spectral-weight transfer, because Z is equal to one and \bar{G} is zero, just as for *qsGW*. The spectral-weight transfer concept can therefore not explain the consistent underestimation observed for molecules in *scGW*.^{11,13,15,16,51,68}

5.1.3 Self-consistent density

Further insight into the effects of different *GW* approaches on electron correlation may be gained from the study of the self-consistent electron density. To focus on the effects of correlation, we consider in the following differences of the PBE, *scGW*, *scGW*₀, and *qsGW* electron density to the density of a Hartree-Fock calculation using with the same computational parameters. Figure 5 illustrates isosurfaces of these density differences for F₂ (upper panel) and BF (lower panel) with isovalues of 0.05 and 0.01 Å⁻³, respectively. To quantify the difference between the *GW* and the HF densities, we introduce a density difference parameter D defined as:

$$D = \int d\mathbf{r} \left| n^{GW}(\mathbf{r}) - n^{HF}(\mathbf{r}) \right| \quad (13)$$

for which the values for BF and F₂ are also reported in Fig. 5.

For both BF and F₂, *scGW* and *scGW*₀ induce qualitatively similar modifications of the electron density as compared to the Hartree-Fock reference both in shape and magnitude (as quantified by

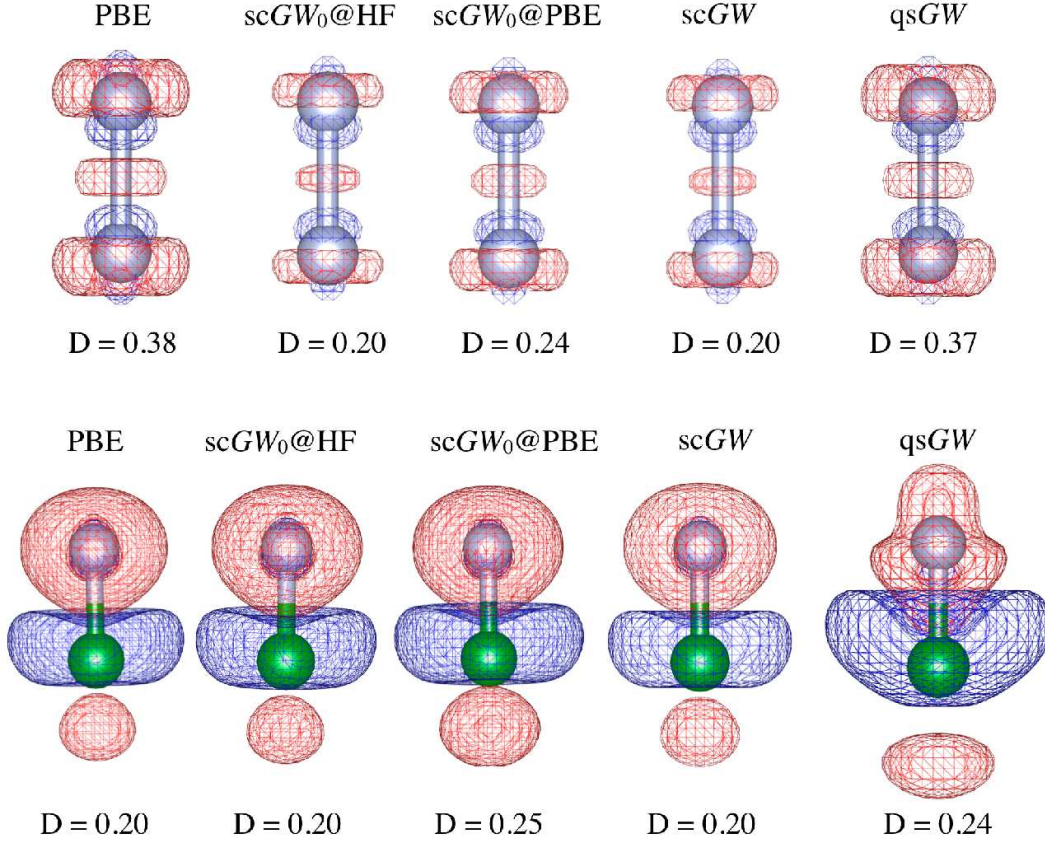


Figure 5: Isosurfaces of the density difference to Hartree-Fock for PBE, $scGW_0@HF$, $scGW_0@PBE$, $scGW$, and $qsGW$. We used an isovalue of 0.05 and 0.01 \AA^{-3} for F_2 (upper panel) and BF (lower panel), respectively.

D). In particular, both $scGW$ and $scGW_0@HF$ yield $D = 0.20$ for BF and F_2 , whereas $scGW_0@PBE$ yields a slight larger modification of the electron density, quantified from the larger D value, which we attribute to over-screening induced by the PBE starting point. In $qsGW$ the change of electron density is more pronounced with respect to $scGW$ and, for the BF dimer, exhibits a considerably different charge redistribution pattern.

Overall, these results indicate that electron densities resulting from $scGW$ and $qsGW$ calculation may exhibit quantitative and qualitative differences. In self-consistent treatments, such density difference affect the external and the Hartree potential as well as the kinetic and the self-energy and thus contribute to the quasiparticle energy difference observed in this work. However, the small example shown in Fig. 5 illustrates that the density difference between $qsGW$ and $scGW$ is neither systematic in shape nor in magnitude and can probably not explain the systematic shift of ~ 0.45

eV observed between our qsGW and scGW data.

5.1.4 Kinetic energy

Another aspect in which scGW and qsGW differ is the treatment of the kinetic energy. In the G_0W_0 approach, the quasiparticles are subject to the non-interacting kinetic energy. If the non-interacting Green's function G_0 derives, for example, from a Kohn-Sham DFT calculation the kinetic energy contribution to the total energy would be that of the *fictitious* non-interacting system of Kohn-Sham particles (T_s). In Kohn-Sham theory, the difference between T_s and the kinetic energy of the interacting system T – as obtained for instance from a self-consistent Green's function calculation – is included through the exchange-correlation energy functional. In the following, we analyze how the kinetic energy is handled in qsGW, a hybrid approach which combines elements of Green's theory and Kohn-Sham theory. In particular, we discuss whether the differences in the scGW and qsGW quasiparticle energies may be ascribed to a different treatment of the kinetic energy in the two methods.

The difference between the non-interacting and the interacting kinetic energy of a GW calculation may be quantified by invoking the analogy with the random-phase approximation (RPA).^{72,73} The total energy in scGW, G_0W_0 , and RPA can be separated into different contributions:^{49,50}

$$E^{GW}[G] = T[G] + E_{\text{ext}}[G] + E_{\text{H}}[G] + E_{\text{x}}[G] + U_{\text{c}}^{GW}[G] \quad (14)$$

$$E^{G_0W_0}[G_0] = T_s[G_0] + E_{\text{ext}}[G_0] + E_{\text{H}}[G_0] + E_{\text{x}}[G_0] + U_{\text{c}}^{GW}[G_0] \quad (15)$$

$$E^{\text{RPA}}[G_0] = T_s[G_0] + E_{\text{ext}}[G_0] + E_{\text{H}}[G_0] + E_{\text{xc}}^{\text{RPA}}[G_0] \quad (16)$$

$$= T_s[G_0] + E_{\text{ext}}[G_0] + E_{\text{H}}[G_0] + E_{\text{x}}[G_0] + E_{\text{c}}^{\text{RPA}}[G_0] + T_{\text{c}}^{\text{RPA}}[G_0] \quad (17)$$

where T is the fully interacting kinetic energy, T_s the non-interacting kinetic energy, E_{ext} the external energy, E_{H} the Hartree energy and E_{x} the exchange energy evaluated for the fully interacting Green's function G or the non-interacting reference calculation G_0 . Following Ref. 49,50, we defined U_{c}^{GW} and $E_{\text{c}}^{\text{RPA}}$ as the correlation energy functionals in the GW and RPA approximation,

respectively:

$$U_c^{GW} = \int_0^\infty \frac{d\omega}{2\pi} \text{Tr}\{v[\chi(i\omega) - \chi_0(i\omega)]\} \quad (18)$$

$$E_c^{\text{RPA}} = \int_0^\infty \frac{d\omega}{2\pi} \int_0^1 d\lambda \text{Tr}\{v[\chi_\lambda(i\omega) - \chi_0(i\omega)]\} \quad (19)$$

where χ_λ is the reducible polarizability

$$\chi_\lambda = \chi_0 + \chi_0 v \chi_\lambda \quad (20)$$

at coupling strength λ that follows from the irreducible polarizability χ_0 defined in Eq. (??). In *GW* there is no coupling strength integration and $\chi = \chi_{\lambda=1}$. RPA contains a coupling strength integration over fictitious systems with coupling strength λ that varies between zero (non-interacting) and one (fully interacting). The comparison between Eq. (??) and (??) reveals that U_c^{GW} contains only electronic correlation (that is, arising from the Coulomb interaction), whereas E_c^{RPA} recaptures a interacting kinetic energy contribution through the coupling constant integration for the same starting point G_0 .⁴⁹ We can then define the kinetic energy contribution of the correlation energy as

$$T_c^{\text{RPA}}[G_0] \equiv E_c^{\text{RPA}}[G_0] - U_c^{GW}[G_0]. \quad (21)$$

Equations (??) to (??) illustrate that both the full Green's function framework (*scGW*) and DFT (e.g., RPA) incorporate the interacting kinetic energy. In the perturbative G_0W_0 framework, however, this contribution is absent.

In *scGW* the quasiparticle energies are extracted directly from the imaginary part of the Green's function, i.e. the spectral function, as illustrated in Section 2, and therefore contain a contribution from the interacting kinetic energy. In DFT, the Kohn-Sham eigenvalues are obtained from the solution of the Kohn-Sham equation. The effective Kohn-Sham potential includes the exchange-correlation potential, that is defined as the functional derivative of the exchange-correlation energy $\frac{\delta E_{xc}}{\delta n}$ and therefore includes the difference between the interacting and the non-interacting kinetic

energy in the correlation potential via the derivative of T_c .

Conversely, in the G_0W_0 approach, the quasiparticle energies ϵ^{QP} are evaluated as a first-order perturbative correction to the single-particle eigenvalues ϵ^{SP} as shown in Eq. (??), which we repeat here for clarity

$$\epsilon_{n\sigma}^{\text{QP}} = \epsilon_{n\sigma}^{\text{SP}} + \langle \psi_n^\sigma | \Sigma^{G_0W_0}(\epsilon_{n\sigma}^{\text{QP}}) - v_{\text{xc}} | \psi_n^\sigma \rangle \quad . \quad (22)$$

For DFT starting points, the matrix element of the exchange-correlation potential v_{xc} subtracts the aforementioned T_c contribution from the eigenvalue $\epsilon_{n\sigma}^{\text{SP}}$. Since $\Sigma^{G_0W_0}$ is purely an exchange and Coulomb correlation self-energy, it does not add an interacting kinetic energy contribution back in, which is thus absent from the G_0W_0 quasiparticle energies.

In *qsGW* the situation is similar to G_0W_0 . Equation (??) is also solved for the *qsGW* quasiparticle energies. However, v_{xc} is replaced by $\tilde{\Sigma}$, the self-consistently determined, optimal, non-local, static potential that best represents the G_0W_0 self-energy. Since $\tilde{\Sigma}$ derives from $\Sigma^{G_0W_0}$ it also does not contain an interacting kinetic energy contribution and neither does $\epsilon_{n\sigma}^{\text{SP}}$. The kinetic energy contribution is therefore also absent from the quasiparticle energies in the *qsGW* framework.

We therefore conclude that although *scGW* and *qsGW* at first glance appear to be similar *GW* self-consistency schemes, they differ quite considerably in their treatment of the kinetic energy. We attribute the observed, average deviation of ~ 0.45 eV between these two schemes to the difference in the kinetic energy treatment, the difference in the electron density and the screening properties.

5.2 Partially self-consistent *GW*

We now turn to the partially self-consistent GW_0 scheme. Unlike *scGW* and *qsGW*, the ionization energies of this partially self-consistent scheme still exhibit a dependence on the starting point, owing to the non-self-consistent treatment of W .¹¹ To account for this dependence, we based our *scGW*₀ calculations on two different starting points: PBE and HF. Our calculations for the *GW*100 set indicate that *scGW*₀@PBE underestimate the ionization energies by 0.34 eV [Fig. 2 (c)], whereas *scGW*₀@HF overestimates them by 0.06 eV [Fig. 2 (d)]. This trend reflects

the over- and under-screening of the screened Coulomb interaction induced by the evaluation of W with PBE or HF orbitals, respectively. In practice, owing to the band-gap problem of Kohn-Sham DFT⁷⁴ PBE calculations typically underestimate the HOMO-LUMO gap by as much as 50% as compared to quantum-chemical calculations or reference experimental values. The small HOMO-LUMO gap, in turn, leads to an overestimation of the polarizability [Eq. (??)] and, correspondingly, of the correlation part of the G_0W_0 self-energy, as alluded to in the previous Section. Conversely, HOMO-LUMO gaps are typically overestimated in Hartree-Fock owing to the lack of electronic correlation which leads, following similar arguments, to an underscreening of the polarizability and a corresponding overestimation of the quasiparticle energies.

The $scGW_0@HF$ and $scGW_0@PBE$ ionization energies differ from each other by 0.4 eV on average, with a maximum deviation of 1 eV (e.g., for F_2Mg). $scGW_0@HF$ exhibits the lowest MAE (0.2 eV) relative to CCSD(T) among the GW methods considered in this work [Fig. 3 (d)]. It gives larger ionization energies than $scGW$ on average. Since also the partial self-consistency scheme incorporates the interacting kinetic energy through the self-consistent Green’s function, we attribute the larger ionization energies in $scGW_0@HF$ to a more pronounced underscreening due to the fact that the HF HOMO-LUMO gap that determines the screening strength of $W@HF$ is larger than that of $scGW$. Conversely, the underscreening in $scGW_0@PBE$ indicates that PBE-based screening ($W@PBE$) is not as suitable for the $GW100$ set as Hartree-Fock based screening ($W@HF$), although for larger molecules or solids, the situation may differ.

5.3 The perturbative G_0W_0 scheme

For comparison, we report in Figs. 2 and 3 the ME and MAE of $G_0W_0@HF$ and $G_0W_0@PBE$. Other G_0 starting points will be discussed in connection to the DSLE-scheme in Section 6. $G_0W_0@PBE$ underestimates the ionization energies by 0.7 eV [Fig. 2 (e)], whereas $G_0W_0@HF$ overestimates by 0.3 eV [Fig. 2 (f)]. G_0W_0 calculations exhibit a more pronounced dependence on the starting point as compared to $scGW_0$, since neither G and W are treated self-consistently. The average discrepancy between $G_0W_0@PBE$ and $G_0W_0@HF$ ionization energies is approximately 1 eV, and

can be as large as 2 eV. For G_0W_0 , in particular, HF provides a better starting point as it leads to a mean absolute error a factor of 2 smaller as compared to PBE [Fig. 3 (e)-(f)]. A similar observation was also made for the ionization energies and electron affinities of organic acceptor molecules.¹³

As alluded to in Section 5.1, $G_0W_0@HF$ gives results that are comparable to $qsGW$. However, $scGW$ differs appreciably. Looking at the progression from $G_0W_0@HF$ to $scGW_0@HF$ to $scGW$ we can now understand the reduction of the ionization energies in terms of changes to the electronic screening, the electron density and the kinetic energy. Going from $G_0W_0@HF$ to $scGW_0@HF$ incurs a density change as illustrated in Fig. 5 and a change from the non-interacting to the interacting kinetic energy (albeit without possible kinetic energy changes due to changes in W). Both effects together reduce the ionization energies on average. Going from $scGW_0@HF$ to $scGW$ does not change the density appreciably anymore according to Fig. 5. The additional reduction of the ionization energies in $scGW$ therefore results from a reduction of the underscreening in W in going from $W@HF$ to the self-consistent W and a concomitant change in the kinetic energy.

5.4 Trends across the $GW100$ set

For all molecules of the $GW100$ set, the deviation from the CCSD(T) ionization energies is illustrated in Fig. 4. The horizontal shaded area marks points differing by less than 0.3 eV from CCSD(T). As a guide through the chemical composition of the different compounds, we divided the $GW100$ set into ten subgroups: atoms, dimers, hydrocarbons, hydrides, halogenides, nitrides, oxides, aromatic molecules, nucleobases, and transition metals compounds. These categories are intended as an approximate indication of the chemical compositions of the $GW100$ subsets. Different categories are color-coded and separated by vertical dotted lines.

Fig. 4 (b) shows that $scGW$ provides accurate ionization energies for molecules of the hydride, halogenide, and oxide groups. The MAE reduces to ~ 0.15 eV if we consider only molecules of the oxide group. A common element of these compounds is the presence of highly electronegative atoms (O, F, Cl) and, correspondingly, the formation of covalent bonds with a strong ionic character. The largest discrepancies among the $scGW$ ionization energies are observed for systems

characterized predominantly by delocalized π -type orbitals such as, e.g., compounds of the hydrocarbon and nucleobase groups. At variance with scGW, scGW₀@HF [Fig. 4 (a)] and G_0W_0 @HF [Fig. 4 (b)] exhibit the largest deviation from CCSD(T) for ionic compounds (hydrides, halogenides, and oxides), whereas the discrepancy is small for π -orbital compounds. Figure 4 further reveals that scGW₀@PBE deviates rather homogeneously from the CCSD(T) reference data.

6 DSLE-min GW ionization energies

We now turn to the discussion of the accuracy of basis-set converged (T4+) DSLE-min GW calculations. In Fig. 6, we report the DSLE for two representative molecules of the GW100 test set, sodium chloride (left) and the adenine nucleobase (right). In practice, the DSLE is estimated by evaluation of Eq. (??) with the QP energies from G_0W_0 @PBEh(α) for α between 0 (pure PBE exchange) and 1 (pure Hartree-Fock exchange). In addition, we show the deviation of the quasi-particle energy for the HOMO from the CCSD(T) reference ($\epsilon_{\text{CCSD(T)}}^{\text{HOMO}} - \epsilon_{\text{QP}}^{\text{HOMO}}$). Both molecules exhibit a clear correlation between the DSLE and the accuracy of the ionization energy. Figure 6 reveals that α values smaller than 0.4 typically result in a positive Δ_{DSLE} and a corresponding underestimation of the ionization energy, whereas the opposite trend is observed for larger α values. At $\alpha \approx 0.4$ for NaCl and $\alpha \approx 0.45$ for adenine we find $\Delta_{\text{DSLE}} = 0$. For NaCl, the DSLE-minimized starting point yields an ionization energy that coincides with the CCSD(T) result, whereas for adenine it is slightly overestimated. More generally, we find for all the systems in the GW100 set that the deviation from CCSD(T) is strongly reduced when the DSLE is minimized.

More generally, we find that also for other systems of the GW100 set the deviation from CCSD(T) is strongly reduced whenever the DSLE is minimized. In Fig. 7, we illustrate the distribution of optimal α values across the systems of the GW100 testset computed with the Tier 4+ basis set. The optimal α determined from the DSLE-min G_0W_0 approach is almost unaffected by finite basis set errors owing to cancellation effects in Eq. (??). Only three molecules of the GW100 testset minimize the DSLE already for $\alpha = 0$ (that is, for pure PBE exchange): LiH, Li₂,

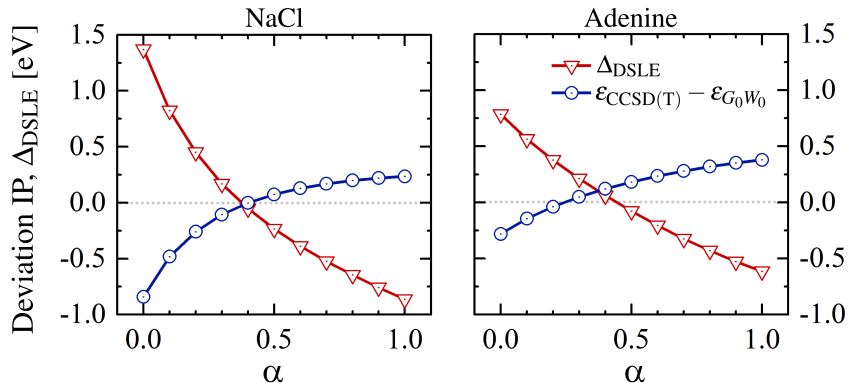


Figure 6: Correlation between DSLE and accuracy of the ionization energy for the NaCl (left) and the adenine (right) molecules. The deviation of the $G_0W_0@PBEh(\alpha)$ HOMO energies from the reference CCSD(T) ionization energies, $\epsilon_{\text{CCSD(T)}} - \epsilon_{G_0W_0}$, is displayed in blue for different amounts of Hartree-Fock exchange α used in the PBE hybrid starting point. The Δ_{DSLE} values are depicted in red as a function of α . We use Tier 4⁺ basis sets for our DSLE-min G_0W_0 calculations.

and Na_2 . The average over all α values amounts to 0.35. This substantiates the results of previous starting-point benchmarks,^{75–78} which find a similar fraction of Fock exchange to provide the most accurate vertical ionization energies. Figure 8 explicitly shows the MAE for the ionization energies of the $GW100$ set obtained from $G_0W_0@PBE(\alpha)$ as a function of α and, marked by a horizontal red line, the MAE of DSLE-min GW .

Finally, in Fig. 8 we report the MAE for the ionization energies of the $GW100$ set obtained from $G_0W_0@PBE(\alpha)$ as a function of α and, marked by a horizontal red line, the MAE of DSLE-min GW . Figure 8 reveals that, among all possible choices of $PBEh(\alpha)$ starting points, the DSLE-minimization procedure yields a gratifying MAE and, thus, is a reliable choice for ionization energy predictions.

7 Conclusions

In summary, we have studied the accuracy of state-of-the-art techniques based on many-body perturbation theory for the description of (charged) electronic excitations in molecules. For compounds of the $GW100$ benchmark set, we have computed the ionization energies as obtained from perturbative (G_0W_0) and self-consistent GW approaches (sc GW , qs GW , and sc GW_0), as well from

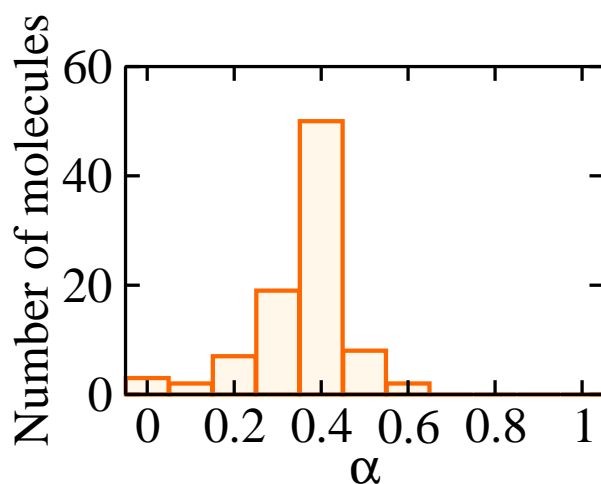


Figure 7: Distribution of the optimal α values obtained from the DSLE-min G_0W_0 approach for the GW100 test set with the Tier 4⁺ basis set.

the recently developed DSLE-min GW approach. Based on the comparison with CCSD(T) reference data, the results presented here quantify the overall accuracy of different flavors of GW calculations for molecular compounds of diverse chemical composition. Overall, our $scGW$ calculations suggest that the effect of vertex correction may become important for compounds characterized by chemical bonds with a pronounced ionic character (as, for instance, halogenides) or by nitrogen-lone pair orbital types, as these compounds exhibit the largest deviation from CCSD(T). Conversely, $scGW$ ionization energies lie typically within 0.3 eV from CCSD(T) for covalently bonded compounds. The comparison between $scGW$, $scGW_0$, and $qsGW$ further reveals that different forms of self-consistency may influence the ionization energies and its agreement with the reference data considerably. We have identified underscreening, density changes and the treatment of the kinetic energy as reasons for the difference in the different self-consistent GW schemes. Finally, we have shown that the deviation from CCSD(T) may in part be attributed to the DSLE and, correspondingly, the DSLE-minimization procedure recently proposed by some of the authors emerges as a promising way to optimize the starting point of G_0W_0 calculations to improve the prediction of ionization energies.

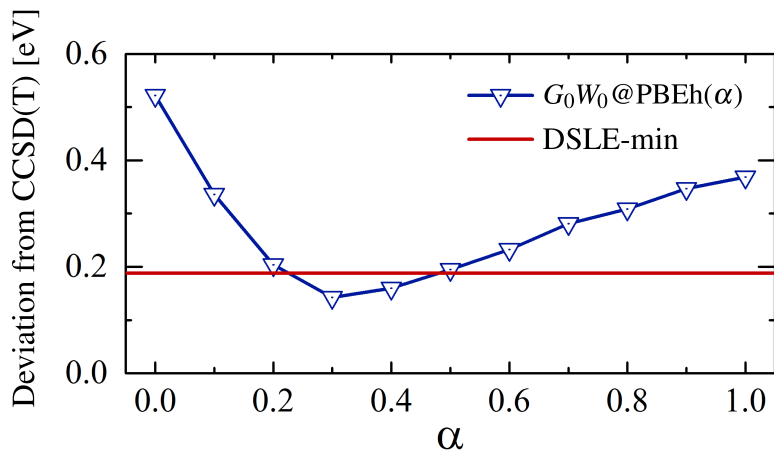


Figure 8: Mean absolute error of the deviation from CCSD(T) for the $G_0W_0@PBE(\alpha)$ ionization energies of the GW100 benchmark set as a function of α . The MAE of DSLE-min GW is reported as a red solid line. We use Tier 4⁺ basis sets for our DSLE-min G_0W_0 calculations.

Acknowledgement

We thank Xinguo Ren and Stephan Kümmel for fruitful discussions. This work was supported by the Academy of Finland through its Centres of Excellence Programme under project numbers 251748 and 284621. M.D. acknowledges support by Deutsche Forschungsgemeinschaft Graduiertenkolleg 1640 and the Bavarian State Ministry of Science, Research, and the Arts for the Collaborative Research Network Soltech.

References

- (1) Fetter, A. L.; Walecka, J. D. *Quantum Theory of Many-Particle Systems*; Dover Publications, 2003.
- (2) Hohenberg, P.; Kohn, W. *Phys. Rev.* **1964**, *136*, B864–B871.
- (3) Kohn, W.; Sham, L. J. *Phys. Rev.* **1965**, *140*, A1133–A1138.
- (4) Aulbur, W. G.; Jönsson, L.; Wilkins, J. W. *Solid State Phys.* **2000**, *54*, 1.
- (5) Onida, G.; Reining, L.; Rubio, A. *Rev. Mod. Phys.* **2002**, *74*, 601–659.

- (6) Rinke, P.; Qteish, A.; Neugebauer, J.; Freysoldt, C.; Scheffler, M. *New J. Phys.* **2005**, *7*, 126.
- (7) Faber, C.; Boulanger, P.; Attaccalite, C.; Duchemin, I.; Blase, X. *Philos. T. R. Soc. A* **2014**, *372*.
- (8) Hedin, L. *Phys. Rev.* **1965**, *139*, A796–A823.
- (9) Hybertsen, M. S.; Louie, S. G. *Phys. Rev. B* **1986**, *34*, 5390–5413.
- (10) Fuchs, F.; Furthmüller, J.; Bechstedt, F.; Shishkin, M.; Kresse, G. *Phys. Rev. B* **2007**, *76*, 115109.
- (11) Marom, N.; Caruso, F.; Ren, X.; Hofmann, O. T.; Körzdörfer, T.; Chelikowsky, J. R.; Rubio, A.; Scheffler, M.; Rinke, P. *Phys. Rev. B* **2012**, *86*, 245127.
- (12) Gallandi, L.; Marom, N.; Rinke, P.; Körzdörfer, T. *J. Chem. Theory Comput.* **2016**, *12*, 605–614.
- (13) Knight, J. W.; Wang, X.; Gallandi, L.; Dolgounitcheva, O.; Ren, X.; Ortiz, J. V.; Rinke, P.; Körzdörfer, T.; Marom, N. *J. Chem. Theory Comput.* **2016**, *12*, 615–626.
- (14) Kaplan, F.; Weigend, F.; Evers, F.; van Setten, M. J. *J. Chem. Theory Comput.* **2015**, *11*, 15152–5160.
- (15) Caruso, F.; Rinke, P.; Ren, X.; Scheffler, M.; Rubio, A. *Phys. Rev. B* **2012**, *86*, 081102.
- (16) Caruso, F.; Rinke, P.; Ren, X.; Rubio, A.; Scheffler, M. *Phys. Rev. B* **2013**, *88*, 075105.
- (17) Faleev, S. V.; van Schilfgaarde, M.; Kotani, T. *Phys. Rev. Lett.* **2004**, *93*, 126406.
- (18) van Schilfgaarde, M.; Kotani, T.; Faleev, S. *Phys. Rev. Lett.* **2006**, *96*, 226402.
- (19) Kaplan, F.; Harding, M. E.; Seiler, C.; Weigend, F.; Evers, F.; van Setten, M. J. *J. Chem. Theory Comput.* **2016**, *12*, 2528–2541.
- (20) Stan, A.; Dahlen, N. E.; van Leeuwen, R. *Europhys. Lett.* **2006**, *76*, 298.

- (21) Stan, A.; Dahlen, N. E.; van Leeuwen, R. *J. Chem. Phys.* **2009**, *130*, –.
- (22) Kutepov, A.; Savrasov, S. Y.; Kotliar, G. *Phys. Rev. B* **2009**, *80*, 041103.
- (23) Rostgaard, C.; Jacobsen, K. W.; Thygesen, K. S. *Phys. Rev. B* **2010**, *81*, 085103.
- (24) Kutepov, A.; Haule, K.; Savrasov, S. Y.; Kotliar, G. *Phys. Rev. B* **2012**, *85*, 155129.
- (25) Koval, P.; Foerster, D.; Sánchez-Portal, D. *Phys. Rev. B* **2014**, *89*, 155417.
- (26) Wang, L.-W. *Phys. Rev. B* **2015**, *91*, 125135.
- (27) Chu, I.-H.; Trinastic, J. P.; Wang, Y.-P.; Eguiluz, A. G.; Kozhevnikov, A.; Schulthess, T. C.; Cheng, H.-P. *Phys. Rev. B* **2016**, *93*, 125210.
- (28) Kotani, T.; van Schilfgaarde, M.; Faleev, S. V. *Phys. Rev. B* **2007**, *76*, 165106.
- (29) Kotani, T.; van Schilfgaarde, M.; Faleev, S. V.; Chantis, A. *J. Phys.: Cond. Mat.* **2007**, *19*, 365236.
- (30) Shishkin, M.; Marsman, M.; Kresse, G. *Phys. Rev. Lett.* **2007**, *99*, 246403.
- (31) Bruneval, F.; Gatti, M. In *First Principles Approaches to Spectroscopic Properties of Complex Materials*; Di Valentin, C., Botti, S., Cococcioni, M., Eds.; Springer Berlin Heidelberg: Berlin, Heidelberg, 2014; pp 99–135.
- (32) Bechstedt, F. In *Many-Body Approach to Electronic Excitations*; von Klitzing, K., Merlin, R., Queisser, H.-J., Keimer, B., Eds.; Springer Series in Solid-State Sciences; Springer, 2015; Vol. 181.
- (33) van Setten, M. J.; Caruso, F.; Sharifzadeh, S.; Ren, X.; Scheffler, M.; Liu, F.; Lischner, J.; Lin, L.; Deslippe, J. R.; Louie, S. G.; Yang, C.; Weigend, F.; Neaton, J. B.; Evers, F.; Rinke, P. *J. Chem. Theory Comput.* **2015**, *11*, 5665–5687.
- (34) Purvis III, G. D.; Bartlett, R. J. *J. Chem. Phys.* **1982**, *76*, 1910.

- (35) Raghavachari, K.; Trucks, G. W.; Pople, J. A.; Head-Gordon, M. *Chem. Phys. Lett.* **1989**, *157*, 479.
- (36) Szabo, A.; Ostlund, N. S. *Modern Quantum Chemistry: Introduction to Advanced Electronic Structure Theory*; McGraw-Hill: New York, 1989.
- (37) Krause, K.; Harding, M. E.; Klopper, W. *Mol. Phys.* **2015**, *113*, 1952–1960.
- (38) Perdew, J. P.; Parr, R. G.; Levy, M.; Balduz, J. L. *Phys. Rev. Lett.* **1982**, *49*, 1691–1694.
- (39) Cohen, A. J.; Mori-Sánchez, P.; Yang, W. *Science* **2008**, *321*, 792–794.
- (40) Atalla, V.; Zhang, I. Y.; Hofmann, O. T.; Ren, X.; Rinke, P.; Scheffler, M. *Phys. Rev. B* **2016**, *94*, 035140.
- (41) Dauth, M.; Caruso, F.; Kümmel, S.; Rinke, P. *Phys. Rev. B* **2016**, *93*, 121115.
- (42) Lani, G.; Romaniello, P.; Reining, L. *New J. Phys.* **2012**, *14*, 013056.
- (43) Lischner, J.; Deslippe, J.; Jain, M.; Louie, S. G. *Phys. Rev. Lett.* **2012**, *109*, 036406.
- (44) Berger, J. A.; Romaniello, P.; Tandetky, F.; Mendoza, B. S.; Brouder, C.; Reining, L. *New J. Phys.* **2014**, *16*, 113025.
- (45) Tandetky, F.; Dewhurst, J. K.; Sharma, S.; Gross, E. K. U. *Phys. Rev. B* **2015**, *92*, 115125.
- (46) Stan, A.; Romaniello, P.; Rigamonti, S.; Reining, L.; Berger, J. A. *New J. Phys.* **2015**, *17*, 093045.
- (47) Scherpelz, P.; Govoni, M.; Hamada, I.; Galli, G. *J. Chem. Theor. Comput.* **2016**, *12*, 3523–3544, PMID: 27331614.
- (48) Dahlen, N. E.; van Leeuwen, R.; von Barth, U. *Phys. Rev. A* **2006**, *73*, 012511.
- (49) Caruso, F.; Rohr, D. R.; Hellgren, M.; Ren, X.; Rinke, P.; Rubio, A.; Scheffler, M. *Phys. Rev. Lett.* **2013**, *110*, 146403.

- (50) Hellgren, M.; Caruso, F.; Rohr, D. R.; Ren, X.; Rubio, A.; Scheffler, M.; Rinke, P. *Phys. Rev. B* **2015**, *91*, 165110.
- (51) Caruso, F.; Atalla, V.; Ren, X.; Rubio, A.; Scheffler, M.; Rinke, P. *Phys. Rev. B* **2014**, *90*, 085141.
- (52) Weigend, F.; Ahlrichs, R. *Phys. Chem. Chem. Phys.* **2005**, *7*, 3297–3305.
- (53) Perdew, J. P.; Burke, K.; Ernzerhof, M. *Phys. Rev. Lett.* **1996**, *77*, 3865–3868.
- (54) Blase, X.; Attaccalite, C.; Olevano, V. *Phys. Rev. B* **2011**, *83*, 115103.
- (55) Faber, C.; Attaccalite, C.; Olevano, V.; Runge, E.; Blase, X. *Phys. Rev. B* **2011**, *83*, 115123.
- (56) Bruneval, F.; Vast, N.; Reining, L. *Phys. Rev. B* **2006**, *74*, 045102.
- (57) Perdew, J. P.; Parr, R. G.; Levy, M.; Balduz Jr, J. L. *Phys. Rev. Lett.* **1982**, *49*, 1691–1694.
- (58) Yang, W.; Cohen, A. J.; Mori-Sánchez, P. *J. Chem. Phys.* **2012**, *136*, –.
- (59) Adamo, C.; Barone, V. *J. Chem. Phys.* **1999**, *110*, 6158–6170.
- (60) Gallandi, L.; Körzdörfer, T. *J. Chem. Theory Comput.* **2015**, *11*, 5391–5400.
- (61) Blum, V.; Gehrke, R.; Hanke, F.; Havu, P.; Havu, V.; Ren, X.; Reuter, K.; Scheffler, M. *Comp. Phys. Comm.* **2009**, *180*, 2175 – 2196.
- (62) Havu, V.; Blum, V.; Havu, P.; Scheffler, M. *J. Comput. Phys.* **2009**, *228*, 8367.
- (63) Ren, X.; Rinke, P.; Blum, V.; Wieferink, J.; Tkatchenko, A.; Andrea, S.; Reuter, K.; Blum, V.; Scheffler, M. *New J. Phys.* **2012**, *14*, 053020.
- (64) TURBOMOLE V7.0 2015, a development of University of Karlsruhe and Forschungszentrum Karlsruhe GmbH, 1989-2007, TURBOMOLE GmbH, since 2007; available from <http://www.turbomole.com>.

- (65) van Setten, M. J.; Weigend, F.; Evers, F. *J. Chem. Theory Comput.* **2013**, *9*, 232–246.
- (66) Liao, P.; Carter, E. A. *Phys. Chem. Chem. Phys.* **2011**, *13*, 15189–15199.
- (67) Bruneval, F.; Sottile, F.; Olevano, V.; Del Sole, R.; Reining, L. *Phys. Rev. Lett.* **2005**, *94*, 186402.
- (68) Pinheiro, M.; Caldas, M. J.; Rinke, P.; Blum, V.; Scheffler, M. *Phys. Rev. B* **2015**, *92*, 195134.
- (69) Holm, B.; von Barth, U. *Phys. Rev. B* **1998**, *57*, 2108–2117.
- (70) Kotani, T.; van Schilfgaarde, M.; Faleev, S. V. *Phys. Rev. B* **2007**, *76*, 165106.
- (71) Schöne, W.-D.; Eguiluz, A. G. *Phys. Rev. Lett.* **1998**, *81*, 1662–1665.
- (72) Langreth, D. C.; Perdew, J. P. *Phys. Rev. B* **1977**, *15*, 2884–2901.
- (73) Ren, X.; Rinke, P.; Joas, C.; Scheffler, M. *Journal of Materials Science* **2012**, *47*, 7447–7471.
- (74) Perdew, J. P.; Levy, M. *Phys. Rev. Lett.* **1983**, *51*, 1884–1887.
- (75) Bruneval, F.; Marques, M. A. *Journal of chemical theory and computation* **2012**, *9*, 324.
- (76) Körzdörfer, T.; Marom, N. *Phys. Rev. B* **2012**, *86*, 041110.
- (77) Körbel, S.; Boulanger, P.; Duchemin, I.; Blase, X.; Marques, M. A. L.; Botti, S. *J. Chem. Theor. Comput.* **2014**, *10*, 3934.
- (78) Govoni, M.; Galli, G. *J. Chem. Theor. Comput.* **2015**, *11*, 2680–2696.

Graphical TOC Entry

